CCFE
CULHAM CENTRE FOR FUSION ENERGY

UK Atomic Energy Authority

UKAEA-CCFE-PR(24)265

P. Ollus, T. Kurki-Suonio, J. Lovell, K. G. McClements,
C. A. Michael, A. Snicker, the MAST-U team1, the
EUROfusion Tokamak Exploitation team

Charge-exchange losses of beam ions in MAST Upgrade: experiments and modelling

Charge-exchange losses of beam ions in MAST Upgrade: experiments and modelling

P. Ollus, T. Kurki-Suonio, J. Lovell, K. G. McClements, C. A. Michael, A. Snicker, the MAST-U team1, the EUROfusion Tokamak Exploitation team

This is a preprint of a paper submitted for publication in Nuclear Fusion

Charge-exchange losses of beam ions in MAST Upgrade: experiments and modelling

P. Ollus[a,*], T. Kurki-Suonio[a], J. Lovell[b], K. G. McClements[c], C. A. Michael[d], A. Snicker[a,e], the MAST-U team[1], and the EUROfusion Tokamak Exploitation team[2]

[a]Department of Applied Physics, Aalto University, P.O. Box 11100, 00076 AALTO, Finland
[b]Oak Ridge National Laboratory, Oak Ridge, TN 37831, USA
[c]United Kingdom Atomic Energy Authority, Culham Campus, Culham Science Centre, Abingdon, Oxon, OX14 3DB, UK
[d]Department of Physics and Astronomy, University of California - Los Angeles, Los Angeles, CA 90095-7099, USA
[e]VTT Technical Research Centre of Finland, FI-02044 VTT, Finland
*Corresponding author
[1]See the author list of J. R. Harrison et al. 2019 Nucl. Fusion, 59 112011
[2]See the author list of "Overview of the EUROfusion Tokamak Exploitation programme in support of ITER and DEMO" by E. Joffrin Nuclear Fusion 2024 10.1088/1741-4326/ad2be4

E-mail: patrik.ollus@aalto.fi (P. Ollus)

27 June 2024

Abstract. Dedicated experiments were performed on MAST Upgrade to study beam-ion losses caused by charge exchange (CX) with edge neutrals. The fuelling was switched from the high-field side to the low-field side mid-discharge. Direct measurements suggest a strong increase in neutral density around the plasma and a deterioration of the beam-ion confinement, which is qualitatively explained by CX. Measurements by a resistive bolometer have suggested particle bombardment during neutral beam injection, providing a unique opportunity to separate CX from other loss mechanisms. To verify and quantify CX losses, the orbit-following ASCOT code was used to simulate beam-particle power loads on the bolometer. Simulations reproduce measured bolometer power loads during high-field-side fuelling, verifying CX losses of approximately 10% of the off-axis beam power. Toroidally symmetric simulations overestimate power loads on the bolometer during low-field-side fuelling, which is explained by toroidal asymmetry in the neutral density distribution, as is demonstrated by toroidally asymmetric simulations. Results suggest significantly higher CX losses during low-field-side fuelling, roughly estimated at 50% of off-axis beam power.

Keywords: fast ions, beam ions, charge exchange, neutral density, toroidal asymmetry, MAST Upgrade, bolometer, ASCOT

1. Introduction

Experiments and modelling have indicated that significant losses of fast ions from neutral beam injection (beam ions) have been caused by charge-exchange (CX) reactions with edge neutrals in the Mega Amp Spherical Tokamak (MAST) and its successor MAST Upgrade (MAST-U) [1, 2, 3]. Moreover, power balance calculations for beam-heated devices have indicated a beam-energy deficit that could be partially explained by CX losses [4]. The observations of beam-ion CX losses in MAST-U motivated dedicated experiments in the 2nd and 3rd experimental campaigns of the device (MU02 and MU03). A key feature in these experiments was that fuelling was switched from the high-field side (HFS) to the low-field side (LFS), which was expected to increase the density of neutrals in the scrape-off layer (SOL) and plasma edge on the LFS. Previous work on MAST-U has shown that, since beam ions in the spherical geometry of the compact device orbit close to the LFS separatrix and have large gyroradii that reach far into the LFS SOL, most of the CX neutralizations that cause losses occur in the LFS SOL [2, 5]. Goals of the present work included verifying that significant CX losses of beam ions occur in MAST-U in its current configuration, identifying plasma scenarios where CX losses should be expected, and quantifying CX losses of beam power.

A range of fast-ion diagnostics was employed to measure the effects of the fuelling switch: a Fast-Ion Deuterium-Alpha (FIDA) [6, 7] system, a Solid-State Neutral-Particle Analyzer (SSNPA) [8] as well as a fission chamber [9] and a neutron camera [10], both of which measure neutron emission. To complement the direct measurements, interpretive modelling was performed using the transport code TRANSP [11, 12]. Since the results of the direct measurements and TRANSP modelling were inconclusive, a more detailed investigation was performed. Measurements from a resistive bolometer suggested particle bombardment caused by CX losses of beam ions [3], providing a unique opportunity to separate CX from other loss mechanisms. To verify and quantify CX losses, the fast-ion orbit-following code ASCOT (5th version) [13, 14] was used to perform modelling tailored for comparison to the bolometer.

The rest of this article is organized as follows. Direct measurements and TRANSP modelling, with a focus on the fuelling switch, are presented in section 2. The quantitative investigation of CX losses through comparison of measured and ASCOT-simulated bolometer power loads is reported in section 3, with considerations of toroidal asymmetry in subsections 3.2 and 3.5. Results are summarized and their implications discussed in section 4.

2. Switching from HFS to LFS fuelling

2.1. Direct measurements

In experiments dedicated to studying beam-ion CX, three double-null L-mode (low-confinement mode) plasma discharges (46735, 49447 and 49452) were performed where the plasma fuelling was switched from HFS to LFS valves. This was intended to introduce additional background neutrals into the LFS SOL and plasma edge, thus increasing CX losses. Figure 1 gives an overview of the discharges, showing plasma current, line-integrated electron density, core electron temperature and neutral-beam power. Only the "off-axis" beam, which injects horizontally 65 cm above the geometric midplane, was used (during times of interest), because particles from the off-axis beam are ionized closer to the edge and, therefore, are more susceptible to CX. Another reason not to use the "on-axis" beam, which injects horizontally in the geometric midplane, was to avoid inducing magnetohydrodynamic instabilities that would make it more difficult to study the effects of CX.

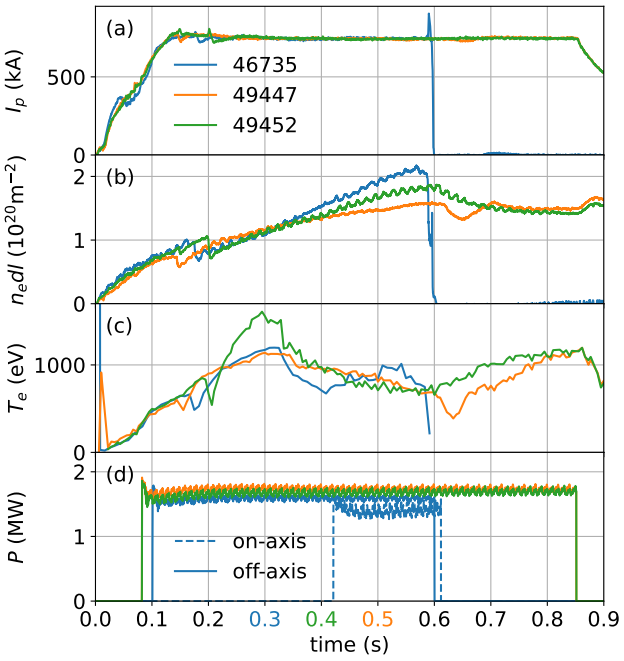

Figure 1: Plasma current (I_p) (a), line-integrated electron density $n_e dl$ (b), core electron temperature (T_e) (c) and neutral-beam power (P) (d) in discharges 46735, 49447 and 49452. Fuelling switch times for the different discharges are indicated by colour-coding of x-axis tick labels.

In discharge 46735, the fuelling switch was programmed to occur at the time 0.30 s, as indicated in Fig. 1. A single midplane LFS fuelling valve was used, the valve in the toroidal sector 9. This valve and other relevant components are indicated

in a top-down illustration of MAST-U in Fig. 2 to aid in describing the experiments and discussing the results. In discharges 49447 and 49452, the same total LFS fuelling rate was used as in discharge 46735, but it was distributed across two midplane LFS fuelling valves, the valves in sectors 9 and 11. The switch was programmed to occur at 0.50 s in discharge 49447 and at 0.40 s in discharge 49452. In all three discharges, a single midplane HFS fuelling valve was used, the valve in sector 2.

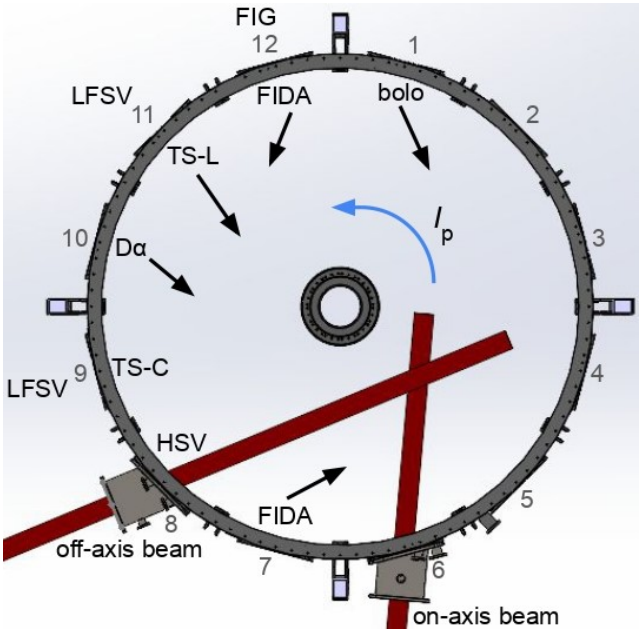

Figure 2: Top-down illustration of MAST-U [8], showing the beam lines and the approximate toroidal locations of the following relevant components: the two LFS fuelling valves (LFSV), the D-alpha diagnostic (Dα), the FIG, the two FIDA views, the Thomson scattering laser (TS-L) and collection system (TS-C), the high-speed-video camera (HSV), and the counter-beam bolometer (bolo). The number designations (1–12) for the toroidal sectors are indicated. Black arrows indicate the approximate orientations of the sightlines of some of the components. A blue arrow indicates the direction of the plasma current (I_p).

Upon switching the fuelling side, immediate effects were observed consistently across the three discharges, as shown in Fig. 3, where the time axis has been normalized to the programmed fuelling switch time. More precise timings were inferred from a midplane D-alpha diagnostic whose sightline overlaps with the fuelling from the LFS valve in sector 9, which was used in all three discharges. As the fuelling gas interacts with the plasma edge, there is a huge increase in the D-alpha signal, as shown in Fig. 3a. In each discharge, the LFS fuelling gas first reached the plasma 5 ms after the programmed fuelling switch time. A strong increase in the neutral pressure, starting approximately 10 ms after the switch time in discharge 49452 and approximately 15 ms after the switch time in discharge 46735, was measured by a Fast Ion Gauge (FIG) [15] at the vacuum vessel wall, as shown in Fig. 3b. The delays may be explained by the time it takes for the fuelling gas to flow to the toroidal location of the FIG and create an increased pressure there. Assuming room temperature (0.025 eV), a deuterium molecule moves at around 1000 m/s, thus traversing the periphery of the vacuum vessel on a timescale of the order of 10 ms. The hypothesis that it takes a finite time for the fuelling gas to spread around the vessel is supported by the slower reaction of the FIG in discharge 46735 than in discharge 49452. The FIG is located in sector 12, and discharge 49452 was fuelled from the valves in sectors 9 and 11 while discharge 46735 was fuelled only from the valve in sector 9. Furthermore, the stronger increase in pressure in discharge 49452, which is also explained by the differing distances from the valves to the FIG, is the first evidence of toroidal asymmetry in the neutral density distribution, which will be discussed in detail in section 3.2. An increase in the neutral pressure at the vessel wall is expected to translate to an increase in the neutral density in the SOL and plasma edge.

Four independent fast-ion diagnostics all measured decreases in signal when the fuelling side was switched, as shown in Fig. 3, panels (c)–(f). Since only the off-axis beam was used, both of the two FIDA views in MAST-U only saw a passive signal. The view from sector 12 overlaps with both of the midplane LFS fuelling valves that were used, as shown in Fig. 2. Like the standard D-alpha diagnostic (Fig. 3a), this FIDA view measured an immediate, huge increase in signal starting 5 ms after the programmed fuelling switch, as shown in Fig. 3c. The corresponding channel in the FIDA view from sector 7, which is roughly on the opposite side of the plasma, shows an immediate, strong decrease in signal followed by a partial recovery over some tens of milliseconds. This is explained by how the FIDA signal is determined by both the fast-ion and neutral densities as well as by how the different processes involved occur on different timescales. The immediate decrease suggests an immediate and substantial decrease in beam-ion density near the plasma edge, i.e. an increase in beam-ion losses. The slower recovery is explained — similarly to the timings in the FIG pressure measurements — by the time it takes for the fuelling gas to move around the vacuum vessel and cause an increase in the neutral density in the SOL region seen by the FIDA view from sector 7. With regard to the production of FIDA light, when the neutral density does increase there, it partially compensates for the decrease in the beam-ion density. In addition

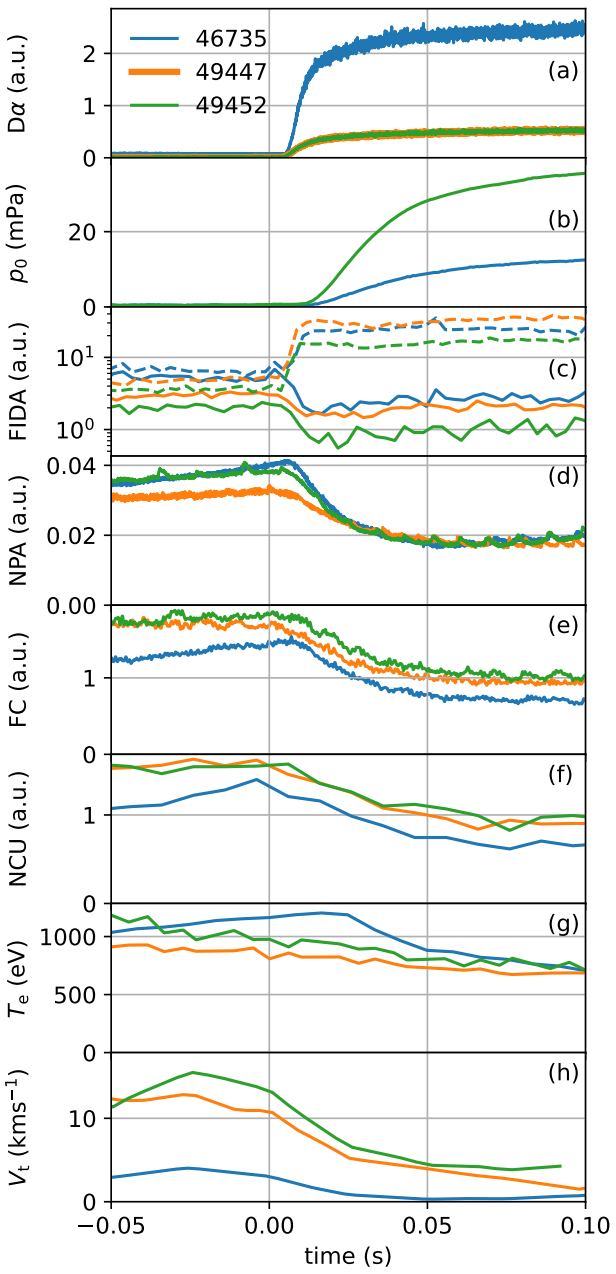

Figure 3: Time traces for the three discharges for the following quantities: midplane D-alpha (a.u.) (a), neutral pressure (mPa) at the vacuum vessel wall (b), FIDA (a.u.) (channel 11 out of 11, which has the largest tangency radius, 1.43 m) from views in sectors 7 (solid) and 12 (dashed) (c), SSNPA (a.u.) (channel 7 out of 48) (d), neutron rate (a.u.) from fission chamber (e), neutron rate (a.u.) from neutron camera (average of all channels) (f), core electron temperature (eV) (g) and plasma rotation as toroidal flow velocity (km/s) at major radius 1.32 m (h). Time abscissae normalized to programmed fuelling switch time. No neutral-pressure data are plotted for discharge 49447 because FIG was not operating.

to FIDA, fast-neutral fluxes measured by the SSNPA (Fig. 3d) as well as neutron emission rates measured by both the fission chamber (Fig. 3e) and neutron camera (Fig. 3f) decreased by about a factor of two within a few tens of milliseconds. All of the decreases in fast-ion diagnostic signals suggest a substantial decrease in beam-ion density, which implies a substantial increase in beam-ion losses caused by the fuelling switch.

It was noted that the central electron temperature, as measured by the core Thomson scattering system [16], decreased notably in discharge 46735, as shown in Fig. 3g. A decrease in temperature shortens the slowing-down time of fast ions, which decreases their density. Therefore, a temperature decrease may be expected to decrease emissions of FIDA light, neutral particles and neutrons, which can complicate the isolation of the impact of a certain loss mechanism. However, the temperature decrease is delayed by 20–30 ms, which is approximately the beam-ion slowing-down time. Hence, the temperature decrease is preceded by and cannot explain the immediate, strong decreases in the fast-ion diagnostic signals starting at 0.305 s. In fact, the decrease in temperature could be a result of beam-ion losses caused by the fuelling switch. Moreover, discharges 49447 and 49452 did not exhibit similar decreases in temperature following the fuelling switch, rather they exhibited slower temperature decreases spanning the full time range of interest. Nevertheless, the temperature decreases may have contributed to the total decreases in the fast-ion diagnostic signals, complicating the investigation of the impact of CX.

It was also noted that the plasma rotation was strongly slowed by the fuelling switch in all three discharges, as shown in Fig. 3h. The toroidal flow velocity was calculated based on measurements by the UCLA Doppler back-scattering system [17] using the equation [18]

$$V_\mathrm{t} = \frac{\omega_\mathrm{d}}{k_\mathrm{p}} \frac{B}{B_\mathrm{p}}, \tag{1}$$

where ω_d is the Doppler shift, k_p is the poloidal component of the scattered wave vector, B is the total magnetic field strength and B_p the poloidal field strength at the point of scattering. Equation (1) implicitly assumes that the Doppler shift is dominated by $\boldsymbol{E} \times \boldsymbol{B}$ rotation (from the radial electric field $\boldsymbol{E}$) and that the turbulence velocity in the plasma rest frame is negligible. It also neglects poloidal rotation considerations, which should be small or at least subdominant [19]. The slowing of the rotation is explained by the drag caused by the interaction between the LFS fuelling gas and the LFS plasma edge. On the one hand, the higher energy of the beam ions in the plasma rest frame is expected to increase the neutron emission. On the other hand,

the decreased shear is expected to decrease energy confinement, resulting in temperature decrease and, by extension, decrease in the beam-ion density. These complex effects further complicate the investigation of the impact of CX.

The beam-ion CX process qualitatively explains the increase in beam-ion losses suggested by the measurements immediately after the fuelling switch. The beam energy was approximately 70 keV. The SOL typically features a neutral temperature of the order of 1–10 eV and a neutral density of the order of 10^{16}–10^{18} m^{-3}. Under such conditions, the CX mean free time is of the order of 10 µs – 1 ms. The slowing-down time of the beam ions was estimated using ASCOT and TRANSP to be 20–40 ms. This is the timescale on which the fast-ion diagnostics are expected to react to changes in plasma parameters, such as density and temperature, due to their effects on the beam-ion density. Beam ions orbit the tokamak toroidally on timescales of 1–10 µs. This means that a toroidally localized influx of neutrals, like those in discharges 46735, 49447 and 49452, can result in CX losses on timescales much faster than other processes, such as the slowing down of beam ions or the movement of fuelling gas around the vacuum vessel. This explains, for example, the initial, immediate decrease in the FIDA signal, followed by a slower partial recovery.

2.2. TRANSP modelling

For an improved understanding of what happened in the plasmas during the switch from HFS to LFS fuelling, TRANSP was used to model the three discharges. TRANSP is suitable for modelling such transient events since the code is designed for time-dependent simulation. There was no attempt to replicate the impact of the fuelling switch on LFS SOL neutral density. The default, fixed SOL neutral density value for TRANSP simulations of MAST-U, $5 \cdot 10^{17}$ m^{-3}, was used throughout the discharges. The aim was to test if the direct measurements discussed in section 2.1 might be reproduced without directly accounting for the change in neutral density. TRANSP was run without any anomalous diffusion.

The total neutron emission estimated by TRANSP features similar relative drops as measured by the fission chamber, as shown in Fig. 4. Since there is significant absolute discrepancy, the TRANSP signal has been scaled to the measurement based on the average values from the 20 ms leading up to the programmed time of the fuelling switch. There appear to be fluctuations and noise in both the measured and simulated signals, so it is difficult to make more detailed comparisons. However, at least in discharges 46735 and 49447, while TRANSP reproduces distinct drops in the neutron emission, the simulated, relative drops are slightly delayed and not quite as strong as the measured. This suggests that part of the change in the beam-ion distribution function is unaccounted for.

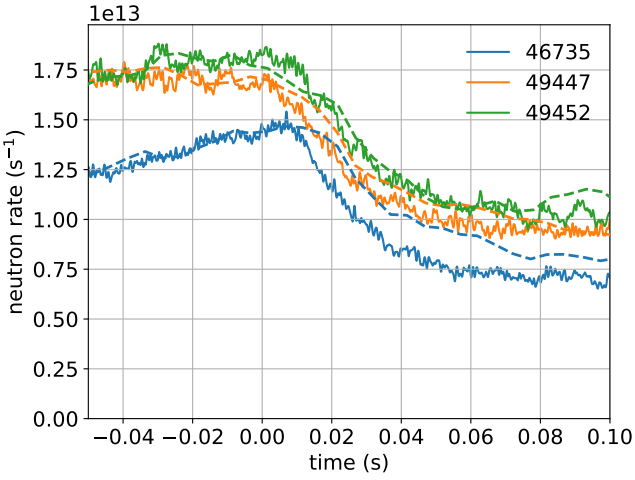

Figure 4: Total neutron emission measured by fission chamber (solid) and simulated by TRANSP (dashed) for the three discharges. TRANSP signal has been scaled to measurement based on average values from the 20 ms leading up to the programmed fuelling switch time (-0.02–0.00 s).

Inspection of the TRANSP results reveals explanations for the simulated drop in neutron emission in the time period following the fuelling switch. As shown in Fig. 5, the plasma density increases (Fig. 5a), which moves the beam-ion birth profile radially outwards (Fig. 5c). In terms of the radial birth rate, this effect appears minor in discharges 49447 and 49452, and more pronounced only in discharge 46735. However, the simulated direct orbit losses increase substantially in all three discharges. Moreover, the plasma temperature decreases (Fig. 5b). It should be noted that the TRANSP modelling was interpretive, meaning that temperature and other plasma parameters are based on measurements. Both the increase in plasma density and decrease in plasma temperature shorten the beam-ion slowing-down time, which, together with the increased direct orbit losses, decreases the beam-ion density. Indeed, TRANSP estimates that the beam-ion density decreases substantially during the 80 ms following the fuelling switch, as shown in Fig. 5d.

These TRANSP modelling results appear to provide alternative explanations for the decreases in the fast-ion diagnostic signals. Direct measurements and TRANSP modelling alone do not reveal the role of CX. Another approach was needed to verify and quantify CX losses.

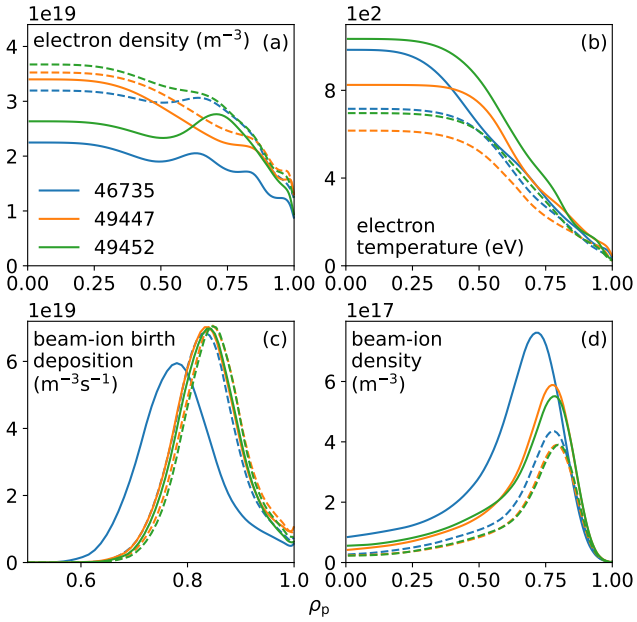

Figure 5: Collection of relevant radial profiles from TRANSP before (solid) and after (dashed) the fuelling switch for the three discharges. For discharge 46735, data are shown for times 0.26 s and 0.38 s. For 49447, 0.46 s and 0.58 s. For 49452, 0.36 s and 0.48 s. Abscissa ρ_p is square root of normalized poloidal flux (section 3.3).

3. Quantifying CX losses using a bolometer

3.1. High bolometer power loads

Although bolometers are designed to detect electromagnetic radiation, energetic particles other than photons can contribute to bolometer signals [3]. During beam injection in MAST-U, the counter-beam channels of an array of resistive bolometers that view the midplane tangentially measure signals an order of magnitude higher than the co-beam channels, as has been reported for experiments of the 1st MAST-U campaign (MU01) [3]. The co-beam signals are on the level expected from the electromagnetic radiation that the diagnostic is designed to measure.

The high bolometer signals, given that they appear during beam injection and only in channels directed counter to the beam injection, suggest bombardment by beam particles. Given the distance of the bolometer from the LFS separatrix, over 30 cm from the closest point on the aperture, charged particles cannot be expected to reach the bolometer. Fast CX neutrals can be expected to reach it.

In the MU02 and MU03 discharges analyzed in the present work, high signals were measured by channel 29, the outermost channel of the counter-beam bolometer, as shown in Fig. 6. This suggests that channel 29 was subject to substantial bombardment by fast CX neutrals, while channels 30–32, the rest of the counter-beam bolometer channels, were subject to only a little bombardment or none at all. The off-axis beam injected practically for the full durations of the discharges: 0.08–0.58 s in discharge 46735 and 0.08–0.85 s in discharges 49447 and 49452. The measured bolometer signals have been heavily smoothed in time, so changes in a signal may have occurred faster in reality than is implied by the graph [3].

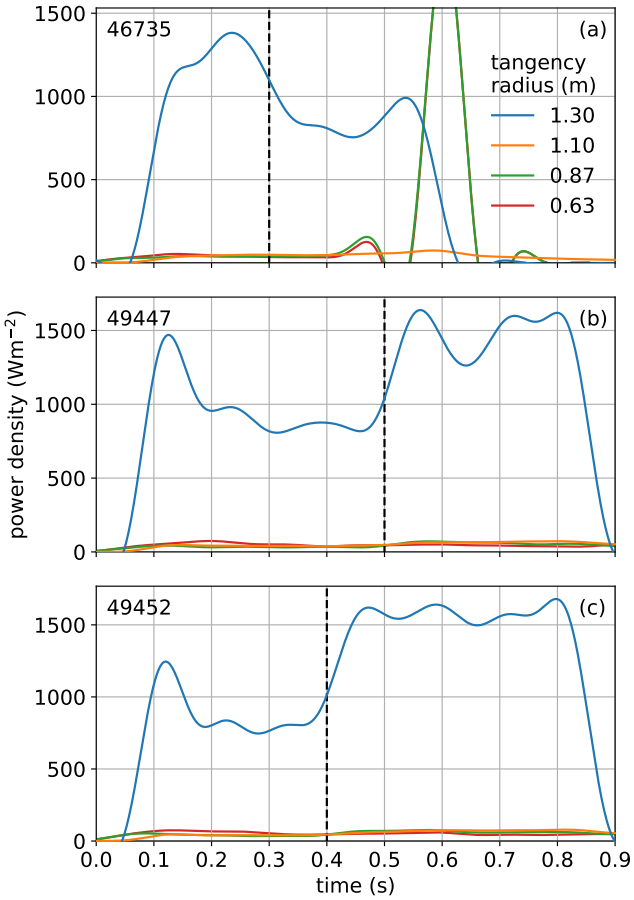

Figure 6: Measured power loads on counter-beam bolometer channels (channels 29–32, with tangency radii 1.30, 1.10, 0.87 and 0.63 m, respectively) as functions of time for the three discharges. Time points for switch from HFS to LFS fuelling indicated by black dashed lines. Signals are heavily smoothed in time. The peaks and troughs in the signals of channels 31 and 32 in discharge 46735 at around 0.6 s are ignored, since they are artefacts of the smoothing algorithm on the radiation spike in the plasma core when it disrupted.

Two additional observations were made about the bolometer measurements shown in Fig. 6. In discharge 46735, the on-axis beam was turned on at around 0.4 s, and the plasma disrupted at around 0.6 s. The modest increase in the bolometer signal of channel 29 during the on-axis beam injection before the disruption

suggests that CX causes losses of beam ions from the on-axis beam as well, although fewer than from the off-axis beam. This is expected, since the off-axis beam deposits ions closer to the edge on average. In discharges 49447 and 49452, the LFS fuelling was turned off 200 ms after being turned on, and the HFS fuelling was not turned back on, leaving the plasmas unfuelled for the remainder of their lifetimes. Yet, the higher bolometer signals, first caused by the switch to LFS fuelling, are maintained after fuelling is turned off. This suggests that the higher neutral density in the plasma region viewed by the counter-beam bolometer is maintained without continued LFS fuelling, likely due to recycling processes. Further investigation of these additional observations is left to future work.

3.2. Toroidal asymmetry

It was qualitatively confirmed that the neutral density around the plasma is toroidally asymmetric during LFS fuelling. Figure 7 shows D-alpha radiation from the three discharges before and after the fuelling switch, as recorded by a high-speed-video (HSV) camera [20], which views the plasma from sector 8 (Fig. 2). The asymmetric brightness distributions after the switch show that LFS fuelling using the valves in sectors 9 and 11, or only the valve in sector 9, gives rise to a toroidally asymmetric neutral density around the plasma.

By considering the toroidal positions of the various elements in the experiments (Fig. 2) and the toroidal asymmetry they produce, certain features of the bolometer measurements shown in Fig. 6 can be qualitatively explained. In discharge 46735, where only the LFS fuelling valve in sector 9 was used, the fuelling switch results in a decrease in the bolometer signal in channel 29. In discharges 49447 and 49452, where valves in sectors 9 and 11 were used, the switch results in an increase in the bolometer signal. The counter-beam bolometer channels, whose aperture is in sector 1, view a region spanning sectors 1–5, i.e. approximately the opposite side of the plasma torus from sector 9. The LFS neutral density probably increases everywhere around the plasma when switching to LFS fuelling valves (Fig. 7), but the beam power remains the same. Since the beam-ion population can be depleted, the toroidal asymmetry of the neutral density after switching to LFS fuelling can result in an increase in CX losses in some toroidal regions and in a decrease in others. A possible explanation for the bolometer measurements is then as follows. The valve in sector 11 causes enough of an increase in the neutral density at the bolometer sightlines compared to elsewhere around the plasma that the bolometer sees an increase in fast CX neutrals escaping in discharges 49447 and 49452. Conversely, when fuelling solely from sector 9 in discharge 46735, the increase in neutral density at the bolometer sightlines is so low compared to around sector 9 that the beam-ion population is largely depleted by CX losses near sector 9, resulting in a decrease in CX losses at the bolometer sightlines. Indeed, as was mentioned in section 2.1, the pressure increase measured by the FIG in sector 12, i.e. between the fuelling valves and bolometer sightlines, is larger in discharge 49452 than in discharge 46735 despite equal

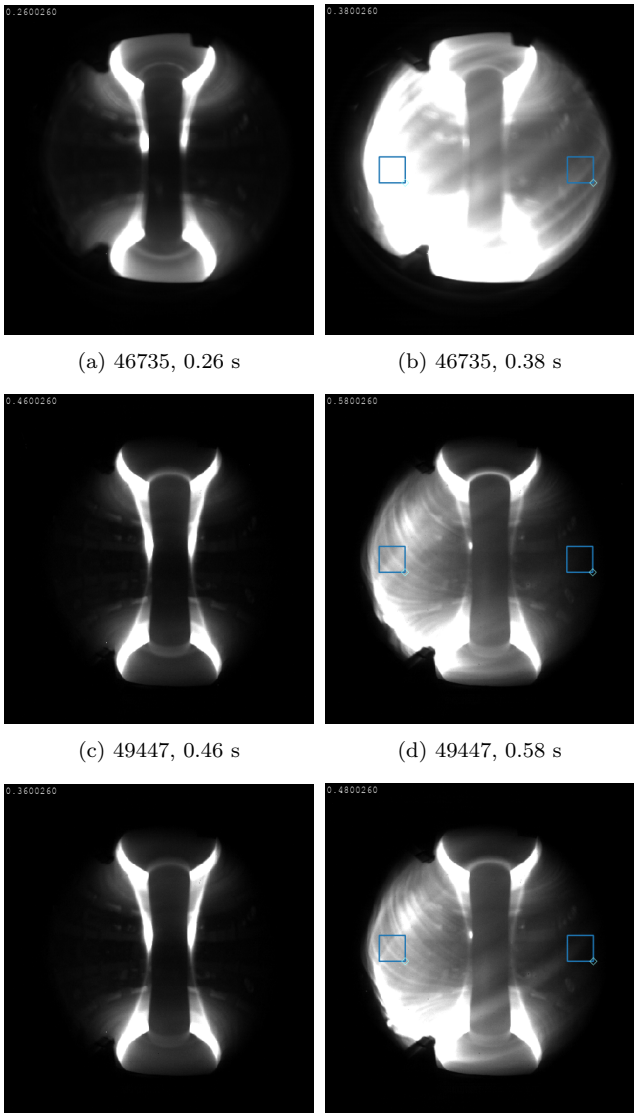

(a) 46735, 0.26 s (b) 46735, 0.38 s

(c) 49447, 0.46 s (d) 49447, 0.58 s

(e) 49452, 0.36 s (f) 49452, 0.48 s

Figure 7: D-alpha radiation during HFS fuelling (a, c, e) and during LFS fuelling (b, d, f) in the three discharges, as recorded by an HSV camera. Sectors 9 and 11, where the LFS fuelling valves reside, are to the left in these images. Discharge number and time point are given for each case. Blue squares indicate averaging areas used when estimating maximum and minimum brightnesses in section 3.5.

total fuelling rates (Fig. 3b).

It was observed that the Thomson scattering measurements indicated significant plasma density in the SOL in the three discharges during LFS fuelling. This is suspicious, especially given that the Thomson scattering system is located near the LFS fuelling valves. The Thomson scattering laser fires from sector 11, where one of the LFS valves is located, while the collection is done from the nearby sector 9, where the other LFS valve is located (Fig. 2). The inferred, possibly false SOL plasma would influence the modelling of beam attenuation and the neutral-density reconstruction. Even if the measurement of plasma density in the SOL is physical, it may well be a toroidally localized phenomenon that should not have an effect elsewhere around the plasma, for example at the beam injection location. The suspicion of phantom plasma in the SOL gives reason to review the reconstruction of kinetic profiles in the plasma edge and SOL during LFS fuelling. However, this non-trivial task goes beyond the scope of this study.

3.3. Simulating bolometer power loads using ASCOT

Since charged particles cannot be expected to reach the bolometer, the high power loads measured on the bolometer provide a unique opportunity to investigate CX losses, isolated from other loss mechanisms. A scheme was devised to simulate the phenomenon using ASCOT to verify the reason for the high bolometer signals as well as to quantify the suspected CX losses. ASCOT is suitable for such modelling since the code follows particles all the way to the device wall.

The target surfaces of the bolometer diagnostic are rectangular foils that are 1.3 mm wide and 3.8 mm high. These foils correspond to the channels (Fig. 6) of the diagnostic. There are four foils inside an aperture with an opening tangentially towards the plasma. The geometry and other technical details of the MAST-U bolometer system have been reported previously, complete with illustrations [3]. Radiation and particles emitted from the plasma must travel through the opening in the aperture to reach a foil. The high bolometer signals were observed only in channels directed counter to the beam injection, i.e. clockwise when viewing the tokamak from above. This is expected from the beam-ion CX effect, which is anisotropic, unlike the electromagnetic radiation that the bolometer is designed to measure. The co-beam bolometer channels were omitted from the simulations for this study. The counter-beam channels have the number designations 29–32 and tangency radii of 1.30, 1.10, 0.87 and 0.63 m, respectively.

A CAD (Computer-Aided Design) model of the counter-beam bolometer diagnostic was included in a virtual 3D reconstruction of the MAST-U wall [5]. Since the bolometer foils are small targets for the markers (test particles) in an ASCOT simulation of the entire tokamak, statistics was a challenge. To improve statistics, copies of the bolometer model were placed all around the tokamak by varying the toroidal angle of the position. Toroidal symmetry was assumed at this stage, although the assumption is false during LFS fuelling, as was discussed in section 3.2. Toroidal asymmetry is simulated in section 3.5. A total of 360 bolometer copies were used, with uniform toroidal spacing, effectively increasing the target area by a factor of 360. Figure 8 shows a part of the ring of virtual bolometer copies, both from the front (Fig. 8a) and from above (Fig. 8b). In Fig. 8a, the foil corresponding to channel 29 can be seen through the openings in the apertures, and, in Fig. 8b, the positions of all four foils in the x-y plane are indicated. Despite tightly packed bolometer copies, apertures did not obscure any sightlines through the openings of neighbouring apertures to their corresponding foils. Given the distance of the bolometer from the plasma, charged particles following curved trajectories to the foils were not expected. Irrelevant support structures of the aperture model were omitted to avoid unnecessary overlapping structures in the final wall model.

ASCOT, with its model for fast-ion CX reactions [2, 5], was used to simulate populations of beam ions under the effect of CX reactions to model fast CX neutrals hitting the counter-beam bolometer foils. For each of the three discharges, 46735, 49447 and 49452, simulations were performed 40 ms before and 80 ms after the programmed time of the fuelling switch, when the plasma density and temperature as well as the magnetic equilibrium were in relatively steady states. To generate the beam-ion populations for the ASCOT simulations, 20 million markers (test particles) were simulated for each case using the BBNBI code [21] (version corresponding to ASCOT5) from the ASCOT suite of codes that models the attenuation of a neutral beam in a plasma. The beam-ion populations were represented by a little fewer than 20 million markers, because those that ended up as shine-through were omitted. In the six cases simulated, the shine-through was 9–16% of the injected beam power. As discussed in section 3.2, during LFS fuelling, the possibly overestimated plasma density in the SOL caused unusually high beam attenuation in the SOL.

The density and temperature of background neutrals, key in CX modelling, were reconstructed on the outer midplane using the 1D kinetic neutral transport code KN1D [22, 23], which takes as input the electron density and electron and ion temperatures as well as the neutral pressure at the vessel wall. Thomson scattering measurements of electron density

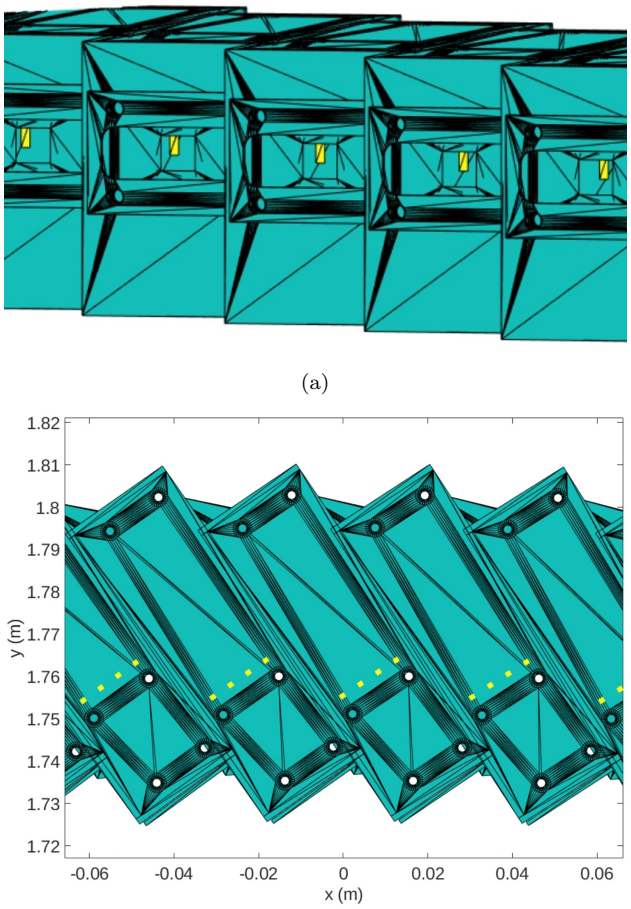

Figure 8: Part of the ring of 360 copies of the counter-beam bolometer model that was used in ASCOT simulations, as viewed from the front (a) and above (b). In (a), the foil (yellow) corresponding to channel 29 can be seen through the openings in the apertures. In (b), the axes display standard machine coordinates, and the positions of all four foils (yellow) in the x-y plane are indicated (would in reality be obscured by aperture roof).

and temperature were used. As discussed in section 3.2, during LFS fuelling, the possibly overestimated electron density in the SOL affected the neutral density reconstruction. The ion temperature was assumed equal to the electron temperature, since the on-axis beam was not used and consequently there were no ion temperature measurements. In MU03 discharges with both beams, the ion temperature measured using charge-exchange recombination spectroscopy [24] tended to be within 50% of the electron temperature, and the fast-particle atomic reactions are insensitive to temperature [5]. The density and temperature profiles were smoothed using a profile-fitting code that fits basis-function splines to the measured data [25]. The neutral pressure at the wall was measured using a midplane FIG. Since the FIG was not operating in discharge 49447, the measurement of the similar discharge 49452 was used as a proxy, shifted by 100 ms like the programmed fuelling switch time. These two discharges were programmed to be exactly the same, with the exception of the 100 ms shift in the timing of the fuelling switch. The claim of similarity is further supported by the overlapping D-alpha measurements shown in Fig. 3a. Since ASCOT cannot yet model CX with molecules, the atomic and molecular densities estimated by KN1D were summed and approximated as a purely atomic neutral background. This is a good approximation when modelling beam-ion CX, as has been argued previously [2]. The temperature for the combined neutral density was calculated as the density-weighted average of the atomic and molecular temperatures estimated by KN1D. Beam-halo neutrals were omitted from the modelling, since only the off-axis beam was used, meaning the beam halo formed around 65 cm above the midplane. CX neutrals travelling through the opening in the bolometer aperture and hitting the foils would have to be born on the midplane. Furthermore, since the beam-halo neutral density is low compared to the density of neutrals coming in from outside the plasma, this omission is not expected to have a significant impact on the total CX losses. At this stage, the neutral density and temperature in the plasma and SOL were assumed to be poloidally and toroidally uniform and were defined as 1D functions of the flux coordinate $\rho_\mathrm{p} = \sqrt{(\psi_\mathrm{p} - \psi_\mathrm{p,ax})/(\psi_\mathrm{p,sep} - \psi_\mathrm{p,ax})}$, where ψ_p is the poloidal flux, and $\psi_\mathrm{p,ax}$ and $\psi_\mathrm{p,sep}$ are its values at the magnetic axis and inside the separatrix, respectively. The poloidal flux was calculated using the EFIT++ code [26, 27] based on magnetic measurements. The neutral density and temperature functions calculated by KN1D were mapped from the major radius to ρ_p on the outer midplane, where the Thomson scattering and FIG measurements were taken. The assumption of a poloidally uniform neutral density based on an outer-midplane reconstruction is considered a good approximation for analysis of beam ions in MAST-U, as has been argued previously [2].

In accordance with the rise in neutral pressure, the reconstructed neutral density profiles are over an order of magnitude higher during LFS fuelling than during HFS fuelling in the three discharges. During HFS fuelling, in the part of the SOL that is reachable by beam ions, the neutral density profiles reach values as high as 7–8·10^{16} m^{-3}. At the separatrix, the values are in the range 2–4·10^{15} m^{-3}, and, inside the confined region of the plasma at $\rho_\mathrm{p} = 0.8$, in the range 1–4·10^{13} m^{-3}. The corresponding ranges of neutral density values during LFS fuelling are 2–5·10^{18} m^{-3}, $7 \cdot 10^{16}$–2·10^{17} m^{-3} and 3–8·10^{14} m^{-3}.

It should be noted that reconstructed neutral

densities for HFS-fuelled plasmas were significantly higher in a previous article on similar work [2]. The reason is that the FIG calibration has progressed since the analysis for the previous article was performed, and neutral pressure measurements give lower values now.

3.4. Toroidally symmetric results

Out of the nearly 20 million markers used in each ASCOT simulation case, a total of the order of tens or hundreds of markers hit the counter-beam bolometer foils. This is enough to get estimates of the power loads on the foils. Table 1 summarizes the simulation results, showing the number of markers that hit each foil in each case as well as the corresponding power load.

Figure 9 shows the measured and simulated power loads on the counter-beam channels of the bolometer during HFS fuelling and during LFS fuelling for the three discharges that were studied. Because of the low statistics of markers hitting bolometer foils in the simulations, noise of the order of some tens of percent should be expected in the simulated power loads on channels 29 and 30, which have tens of hits during HFS fuelling and around a hundred hits during LFS fuelling. On channels 31 and 32, since they tend to have only a few hits, the noise is of the same order as the signal, which explains why a higher neutral density resulted in a lower power load in some cases. Nevertheless, if all three discharges are considered simultaneously to mitigate the noise issue, the results are sufficient to estimate the order of magnitude of the power loads on channels 31 and 32.

The power loads measured on the bolometer foils during HFS fuelling were approximately reproduced in simulations in all three discharges, with the exception of channel 30, as is shown in Fig. 9. In each discharge, the simulated power load on channel 29 agrees with measurement during HFS fuelling to within 40%, as shown in Fig. 9a. The low loads on channels 31 and 32 (Figs. 9c and 9d), if all three discharges are considered simultaneously to mitigate the noise issue, were reproduced during HFS fuelling in the sense that they are an order of magnitude lower than the loads on channel 29. It should be kept in mind, however, that, unlike the simulated power loads, the measured loads also include radiation, which is expected to be on a similar level for all channels as well as both during HFS and during LFS fuelling. Loads on channel 30 (Fig. 9b), both during HFS and during LFS fuelling, and on channel 29 during LFS fuelling were overestimated. Because of the high statistical noise, it is difficult to interpret the simulated loads on channels 31 and 32 also during LFS fuelling, but there appears to be similar relative overestimation for channel 31 as for channel 29 and no overestimation for channel 32.

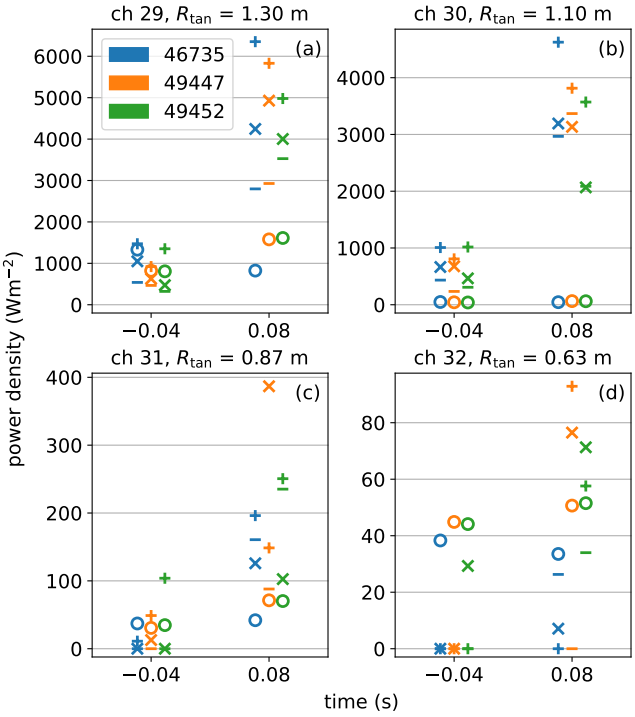

Figure 9: Measured (○) and simulated power load densities on the four counter-beam bolometer channels during HFS (-0.04 s) and LFS (0.08 s) fuelling in the three discharges. Results simulated using the measured (×), halved (-) and doubled (+) neutral pressure are included. Channel ("ch") number and tangency radius (R_{tan}) given above each panel. Time abscissae normalized to programmed fuelling switch time. Data points for discharges 46735 and 49452 are slightly shifted along the time axis, purely for the purpose of readability.

The simulation results were inspected more closely regarding the initial ρ_p-coordinate and final energy of those markers that hit bolometer foils. During HFS fuelling in each discharge, channels 29 and 30 were predominantly hit by markers that had originally been ionized radially further out, i.e. from the outer half of the beam-ion population. During LFS fuelling, channels 29 and 30 were hit by markers from all initial ρ_p-coordinates roughly in proportion to the birth distribution. The full energy spectrum was consistently represented among the markers that hit bolometer foils both during HFS and during LFS fuelling. However, during LFS fuelling, channels 29 and 30 were hit relatively more by markers with higher energies. This complements the preceding observation that LFS fuelling resulted in marker hits also from deeper in the plasma, since such CX neutrals must penetrate more plasma without being reionized, which requires higher energies.

The successful reproduction of the power loads on channels 29, 31 and 32 during HFS fuelling shows that

Table 1: Number of markers that hit each counter-beam bolometer channel ("hits") and resulting estimated power load density ("power", Wm^{-2}) in each simulation case. Cases are specified by discharge number, time point during discharge (s) and whether the measured neutral pressure ("$\times p_0$" = "1") was used when reconstructing the neutral background or half ("0.5") or double ("2") the measured pressure.

		channel	29		30		31		32	
discharge	time (s)	$\times p_0$	hits	power	hits	power	hits	power	hits	power
46735	0.26	0.5	16	539.2	16	434.0	0	0.0	0	0.0
		1	30	1048.7	16	664.8	0	0.0	0	0.0
		2	42	1472.6	29	1008.1	1	11.1	0	0.0
	0.38	0.5	70	2797.6	78	2966.3	5	160.7	1	26.3
		1	106	4244.9	86	3192.8	6	125.9	1	7.1
		2	131	6352.8	109	4625.6	7	196.2	0	0.0
49447	0.46	0.5	15	466.7	7	234.7	0	0.0	0	0.0
		1	17	627.8	15	677.7	1	12.8	0	0.0
		2	29	921.5	22	807.9	1	48.9	0	0.0
	0.58	0.5	77	2927.9	87	3368.1	4	88.0	0	0.0
		1	108	4928.7	77	3134.4	12	386.8	2	76.5
		2	126	5830.5	94	3814.9	5	148.6	2	92.9
49452	0.36	0.5	12	322.4	9	307.7	0	0.0	0	0.0
		1	16	473.4	16	464.8	0	0.0	1	29.3
		2	41	1351.7	32	1017.5	4	103.9	0	0.0
	0.48	0.5	89	3528.0	53	2086.8	7	235.2	2	34.0
		1	84	4002.3	59	2067.5	4	102.6	2	71.3
		2	110	4979.9	86	3571.0	8	250.6	2	57.6

the beam-ion CX process does, indeed, explain the high bolometer measurements. Further, it indicates that the neutral density and other simulation inputs are realistic during HFS fuelling, at least in those plasma regions from which CX neutrals can bombard the bolometer foils. Therefore, the simulations can be expected to provide realistic estimates of the overall impact of CX on the beam-ion population. It is estimated that 9%, 7% and 7% of the beam power that is originally deposited in the plasma is lost due to CX during HFS fuelling in discharges 46735, 49447 and 49452, respectively. Power lost due to CX is here approximated as the power contained in markers that hit the wall as neutrals, which has been deemed a good approximation [2].

It is recognized that accurately reconstructing the neutral background is difficult, whether it be due to inaccuracy in the neutral pressure measurements, inaccuracy in the reconstruction of the plasma density and temperature profiles, or something else. Therefore, the neutral background was not assumed accurate, but a sensitivity scan was performed. The measured neutral pressure was halved and doubled, and the simulations were rerun with the resulting lower- and higher-density neutral backgrounds. The resulting, alternative simulated bolometer power loads are included in Tab. 1 and Fig. 9.

The measured bolometer signal for channel 29 during HFS fuelling consistently falls between the results simulated for the actual, measured neutral pressure and the double pressure (Fig. 9a). This suggests that the neutral density and CX losses are somewhat underestimated when calculated based on the neutral pressure measurement, possibly due to remaining uncertainty in the FIG calibration. The simulated losses of beam power for all three neutral pressures for all six plasma cases are gathered in Tab. 2. Based on the above reasoning, the true value for the loss of beam power due to CX during HFS fuelling is between the estimates from the case with the measured neutral pressure and the case with double pressure, i.e. 9–14%, 7–12% and 7–13% in discharge 46735, 49447 and 49452, respectively. The relatively small increase in CX losses during LFS fuelling when doubling the neutral pressure is explained by depletion of the beam-ion population near the plasma edge.

The extra simulations from the sensitivity scan shed some light on the role of statistical noise in the results. For example, it appears that the simulated power load on channel 29 in discharge 49452 during HFS fuelling, when using the measured neutral pressure, happens to be at the low end of what the simulation might yield (Fig. 9a). A rerun with different random seeds would likely yield a power load closer to the midpoint between the power loads simulated for the half and double neutral pressures in the same plasma case. Assuming Poisson noise, where the error is the square root of the number of hits,

Table 2: Simulated loss of beam power (excluding shine-through) due to CX (hit the wall as a neutral) in each case. Cases are specified by discharge number, time point (s) and whether the measured neutral pressure ("$\times p_0$" = "1") was used when reconstructing the neutral background or half ("0.5") or double ("2") the measured pressure.

			power loss	
discharge	time	$\times p_0$	MW	%
46735	0.26	0.5	0.07	5
		1	0.12	9
		2	0.19	14
	0.38	0.5	0.38	26
		1	0.53	37
		2	0.69	47
49447	0.46	0.5	0.06	4
		1	0.11	7
		2	0.19	12
	0.58	0.5	0.67	43
		1	0.86	54
		2	1.03	65
49452	0.36	0.5	0.06	4
		1	0.11	7
		2	0.19	13
	0.48	0.5	0.55	36
		1	0.72	47
		2	0.89	58

the 'true' number of hits when using half, measured and double neutral pressure could be 9, 20 and 35, respectively, rather than 12, 16 and 41, as quoted in Tab. 1. Because 20-million-marker simulations are computationally intensive, it was not deemed appropriate to rerun exactly the same simulations just to get several statistical samples for each result. The results obtained from the 18 simulations that were run already provide a clear enough picture.

The overestimation of the power loads on channel 30 and, during LFS fuelling, on channel 29 indicate inaccuracies in the simulation inputs. The neutral density, which is notoriously difficult to reconstruct, is the obvious first candidate. Uncertainty in the Thomson scattering measurements, particularly in the SOL and near the separatrix, upon which not only the neutral density reconstruction but also the beam attenuation depends sensitively, makes the beam-ion birth distribution another likely candidate. As was discussed in section 3.2, the plasma density in the SOL and near the separatrix may have been overestimated during LFS fuelling, causing false ionization of beam particles in these regions. Of such beam ions, those that were ionized on barely confined orbits, because they orbit far out in the SOL and have more radial velocity vectors, are more likely than beam ions that were ionized deeper in the plasma to be neutralized by CX and hit those bolometer foils whose sightlines have lower tangency radii. However, as was discussed above, markers that hit channel 30 tended to have similar initial ρ_p-coordinates as markers that hit channel 29. An overestimated neutral density would explain more marker hits on all channels. It is suspected that the neutral density during LFS fuelling was overestimated in the simulations reported on in this section, as will be discussed below. The overestimation of the load on channel 30 during HFS fuelling could also be caused by a mismatch in the absolute positioning of the physical and virtual bolometers.

In this section, the ASCOT modelling did not account for toroidal asymmetry in the neutral density, which may explain why the power loads on the bolometer were overestimated during LFS fuelling. This hypothesis is supported by how the discrepancy between measured and simulated bolometer loads (Fig. 9) is greater in discharge 46735, which only used the LFS fuelling valve in sector 9, than in discharges 49447 and 49452, which also used the valve in sector 11, which is closer to the region viewed by the bolometer (Fig. 2). The ASCOT neutral density input assumed a global increase in line with the pressure measurement in the one operating main-chamber FIG, which is in sector 12. In the case of discharges 49447 and 49452, since one of the LFS fuelling valves used is in sector 11, close to the FIG, a neutral density estimate based on a measurement by the FIG not only fails to reproduce the toroidal asymmetry but also is likely an overestimation of the average neutral density around the plasma. Hence, the simulations for time periods during LFS fuelling in these two discharges were not only incapable of accounting for the toroidal asymmetry but also likely overestimated the total CX losses. Accurately simulating fast CX neutrals hitting the bolometer during LFS fuelling would require a reconstruction of the toroidally asymmetric neutral density. While accurately modelling the toroidal asymmetry goes beyond the scope of this article, a first study on the impact of a toroidally asymmetric neutral density distribution was performed and is reported in section 3.5.

3.5. Toroidally asymmetric results

To test the hypothesis that the overestimation of bolometer loads during LFS fuelling in section 3.4 is due to toroidal asymmetry, proof-of-principle-level toroidally asymmetric modelling was performed. The cases with LFS fuelling, i.e. discharge 46735 at 0.38 s, discharge 49447 at 0.58 s and discharge 49452 at 0.48 s, were simulated using ASCOT with simple toroidally non-uniform neutral density distributions. Realistically reconstructing the toroidal asymmetry in the neutral density is a challenging undertaking and is

left to future work.

The 1D neutral background data described in section 3.3 was mapped to a 3D grid, and the density was made non-uniform in the toroidal angle based on a simple, empirical model. The neutral density distribution was assumed to have its maximum at the toroidal location of the fuelling epicentre and its minimum at the opposite side of the plasma torus, and the density function was assumed linear in the toroidal angle. In discharge 46735, the fuelling epicentre was the location of the one fuelling valve that was used, the valve in sector 9 (Fig. 2). In discharges 49447 and 49452, the epicentre was the midpoint between the two valves that were used, the valves in sectors 9 and 11. Toroidal locations of components were approximated as the midpoints of the sectors where they reside. For each case, the absolute value of the neutral density was determined based on the corresponding 1D neutral density profile such that the density of the 3D neutral background matched the density of the 1D neutral background at the toroidal location of the FIG (sector 12). The 1D neutral background based on the measured neutral pressure was used. The sensitivity scan was not repeated, since the focus here is on the impact of the toroidal non-uniformity of the neutral density distribution. The neutral temperature was left uniform in the toroidal angle.

The D-alpha brightness data from the HSV camera (Fig. 7) was used to estimate the ratio between the maximum and minimum neutral density values along the toroidal angle during LFS fuelling. If it is assumed that metastable states due to electron excitation dominate over metastable states due to recombination and charge-exchange reactions, the latter two can be neglected and the D-alpha emissivity can be calculated as [28]

$$\epsilon_{3\to 2} = \mathrm{PEC}^{(\mathrm{exc})}_{3\to 2} n_e n^0_D, \tag{2}$$

where $\mathrm{PEC}^{(\mathrm{exc})}_{3\to 2}$ is the excitation photon emissivity coefficient (depends on electron density and temperature) for the transition from the energy state $n = 3$ to $n = 2$ (n is the principal quantum number), n_e is the electron density and n^0_D is the neutral-deuterium density. Based on eq. (2), the brightness is proportional to the neutral density when the electron density and temperature remain fixed. Therefore, the ratio between the maximum and minimum neutral density values can be estimated as the ratio between the maximum and minimum brightnesses. The maximum and minimum brightnesses were estimated as the average brightnesses inside small squares on the left and right sides, respectively, of the HSV image. The squares are indicated in Figs. 7b, 7d and 7f. The ratios evaluated for discharges 46735, 49447 and 49452, during LFS fuelling, are approximately 3.4, 13 and 13, respectively.

The lower brightness ratio in discharge 46735 may be explained by the point of minimum brightness being further behind the plasma on the right side of the image (Fig. 7b) than for discharges 49447 and 49452 (Figs. 7d and 7f). The HSV camera views the plasma from sector 8, so it makes for a substantial difference whether the full fuelling rate comes from the adjacent sector 9 or that same fuelling rate is evenly distributed between sectors 9 and 11. Another reason that the brightness ratio for discharge 46735 may be underestimated is that Fig. 7b appears to be saturated on the left side.

Adequate statistics for toroidally resolved marker hits on bolometer foils were not possible. Instead, the toroidally resolved deposition of CX neutrals on the whole wall was the quantity of interest in this modelling of the toroidal asymmetry. To save on computational resources, fewer markers were used for these simulations than in section 3.3. BBNBI was run with 2 million markers to generate beam-ion populations for each of these ASCOT simulations.

The toroidally non-uniform neutral density distribution gave rise to a toroidally non-uniform power deposition on the wall from CX losses, again approximated as the power contained in markers that hit the wall as neutrals. Figure 10 shows the toroidally resolved neutral density at the separatrix and power deposition from fast neutrals to the wall during LFS fuelling. The data resulting from the use of toroidally uniform neutral density distributions during LFS fuelling as well as the data for the cases during HFS fuelling (toroidally symmetric) are also shown for comparison. In the toroidally non-uniform cases, the maximum power deposition is shifted from the maximum neutral density in the positive toroidal direction, which is explained by how the beam injects tangentially in the positive toroidal direction. The modest fluctuations in the power-deposition graphs compared to the neutral-density graphs are likely due to protruding components in the 3D wall.

The results in Fig. 10 verify the hypothesis that the overestimation of bolometer power loads during LFS fuelling in section 3.4 is explained by toroidal asymmetry. In discharges 49447 and 49452, in the region viewed by the bolometer, i.e. sectors 1–5 (shaded in Fig. 10), the power loads resulting from the toroidally non-uniform neutral density are 1–4 times lower than the loads resulting from the toroidally uniform neutral density. In section 3.4, the bolometer loads on channel 29 in discharges 49447 and 49452 were overestimated by a factor of 2–3 (2–4 when including sensitivity scan) during LFS fuelling. In discharge 46735, since the power deposition simulated during LFS fuelling with the toroidally non-uniform neutral density is not lower than the power deposition

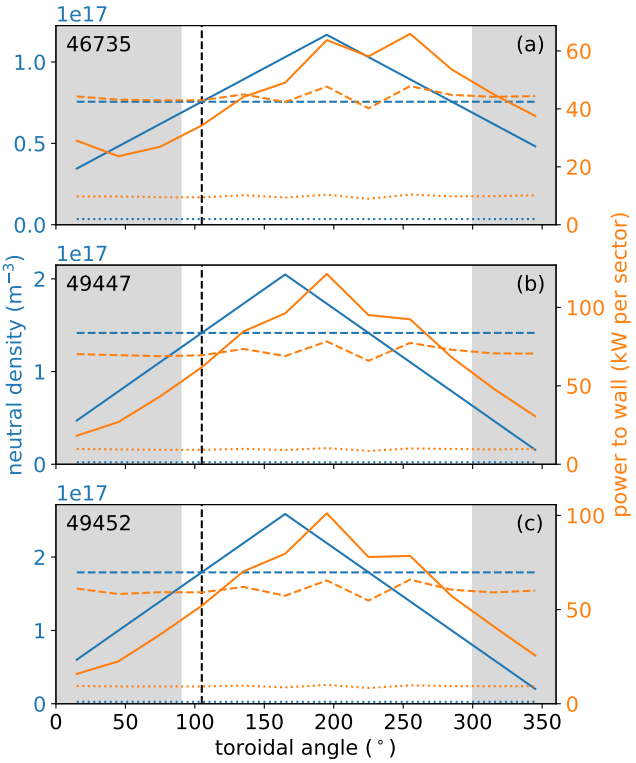

Figure 10: Neutral density at the separatrix (blue) and power deposition from fast neutrals to the wall (orange) in the three discharges, during LFS fuelling, simulated both using toroidally non-uniform (solid) and toroidally uniform (dashed) neutral density distributions, as well as during HFS fuelling (dotted). Sectors viewed by bolometer indicated by grey shading. Location of FIG indicated by black vertical dashed line. Toroidal coordinate runs counter-clockwise, starting between sectors 3 and 4 (Fig. 2).

simulated during HFS fuelling at any toroidal angle, the measured decrease in the power load on channel 29 (Fig. 6a) is not demonstrated. However, this could be due to underestimation of the full toroidal variation of the neutral density because of the HSV camera having a poor vantage point for this discharge, as discussed above. Moreover, as discussed above, this modelling of the toroidal asymmetry features several approximations and simplifications, so precise results cannot be expected. The results of this section amount to a proof of principle, explaining the overestimation of the bolometer loads during LFS fuelling, as simulated using toroidally uniform neutral density distributions in section 3.4.

While precise analysis of beam-ion CX during LFS fuelling is not yet possible, the results suggest significantly higher CX losses during LFS fuelling than during HFS fuelling. As expected based on the discussion in section 3.4 about the proximity of the fuelling to the FIG, the total CX losses in discharges 49447 and 49452 were lower using the toroidally non-uniform neutral density distribution, but only slightly lower. Switching from the uniform to the non-uniform neutral density in the 2-million-marker simulations, the losses reduced from 56% to 51% for discharge 49447 and from 47% to 43% for discharge 49452. Similarly as when doubling the neutral pressure during LFS fuelling in section 3.4, the relatively small difference is explained by depletion of the beam-ion population near the plasma edge. In discharge 46735, the total losses remained the same, 35%. This is explained by the FIG being exactly midway between the neutral-density maximum at the LFS fuelling valve in sector 9 and the minimum on the opposite side of the torus in sector 3, since it means that the 1D neutral density is the average of the 3D neutral density along the toroidal angle. The results of section 3.4 and the present section suggest that 40–60% of the beam power that is originally deposited in the plasma is lost due to CX during LFS fuelling.

4. Summary

In response to early results that indicated significant CX losses of beam ions, dedicated experiments were performed in MAST-U to study the phenomenon. In three similar L-mode discharges, featuring only the off-axis neutral beam, the fuelling was switched from HFS to LFS valves to increase the neutral density in the LFS SOL and plasma edge. Direct measurements showed a strong increase in background neutral pressure and indicated a strong decrease in beam-ion density. While the CX process qualitatively explains the observations, TRANSP modelling appeared to provide alternative explanations, highlighting the difficulty in isolating the role of CX. A different approach was needed to verify and quantify CX losses.

The MAST-U bolometer had measured an order of magnitude higher signals than usual during neutral beam injection, although only in the injection direction, indicating particle bombardment. Since charged particles should be unable to reach the bolometer, fast CX neutrals originating from the population of beam ions were suspected. To investigate this hypothesis, the fast-ion orbit-following code ASCOT was used to simulate the population of beam ions in the presence of CX reactions with a model of the bolometer embedded in the virtual 3D wall. The measured power loads on the bolometer were partially reproduced during HFS fuelling, verifying CX losses of approximately 10% of the off-axis beam power (excluding shine-through). Bolometer power loads were overestimated during LFS fuelling, which was suspected to be caused by toroidal asymmetry in the neutral density distribution that could not be

accounted for in the initial modelling. Additional modelling was performed using a simple toroidally non-uniform neutral density distribution. The results demonstrate that toroidal asymmetry explains the overestimated bolometer loads and suggest losses of approximately 50% of the off-axis beam power during LFS fuelling. Precise analysis of LFS-fuelled plasmas is left to future work when the toroidal asymmetry can be accurately modelled or toroidally symmetric LFS fuelling is available. While this study did not include modelling of fast ions from the on-axis beam, an experimental indication of CX losses also from the on-axis beam was noted.

The estimated loss of power due to CX during HFS fuelling, approximately 10%, is comparable to a previous estimate of power imbalance in beam-heated devices, approximately 25% [4], suggesting that CX losses may explain part of the observed power deficit. MAST-U is being upgraded with a cryoplant, which is expected to reduce the background neutral density. The ability demonstrated here to quantify CX power losses not only enables more accurate power balance calculations but also provides a method for gauging the effectiveness of the cryoplant at improving the plasma performance. The evidence provided for increased CX losses during LFS fuelling will help design successful experiments with LFS fuelling. While MAST-U will have more LFS fuelling valves operating in the future, which will reduce the toroidal asymmetry noted in this study, improvements in the reconstruction of the neutral density distribution are envisioned. Such improvements include descriptions of the poloidal and toroidal asymmetries due to recycling from the divertors and the positions of fuelling valves. This will allow quantification of CX losses during LFS fuelling, which will enable more accurate modelling of the impact of CX on beam ions. On a more general note, switching from HFS to LFS fuelling was found to have profound effects on the plasma, e.g. strongly slowing the rotation, which warrants further study towards an improved understanding of LFS-fuelled plasmas.

Acknowledgements

We thank Rory Scannell for help with the FIG, Marco Cecconello for help with the neutron camera, Bhavin Patel for help with TRANSP, Chris Bowman for help with the profile-fitting code, Roy McAdams for help with the neutral beam, and Konsta Särkimäki for help with ASCOT. The ASCOT simulations were carried out on the EUROfusion High Performance Computer, Marconi-Fusion, at CINECA. We acknowledge the computational resources provided by the Aalto Science-IT project. This work has been carried out within the framework of the EUROfusion Consortium, funded by the European Union via the Euratom Research and Training Programme (grant agreement No. 101052200 — EUROfusion) and also with support from the EPSRC [grant No. EP/W006839/1] and the US DoE grant Nos. DE-SC0019005, DE-SC0019007 and DE-AC05-00OR22725. Views and opinions expressed are however those of the author(s) only and do not necessarily reflect those of the European Union or the European Commission. Neither the European Union nor the European Commission can be held responsible for them. This work was partially funded by the Academy of Finland project Nos. 324759, 328874 and 353370.

Data availability statement

The data that support the findings of this study are openly available at ((INSERT DOI)).

References

[1] K.G. McClements, K. Tani, R.J. Akers, Y.Q. Liu, K. Shinohara, H. Tsutsui, and S. Tsuji-Iio. The effects of resonant magnetic perturbations and charge-exchange reactions on fast ion confinement and neutron emission in the Mega Amp Spherical Tokamak. *Plasma Physics and Controlled Fusion*, 60(9):095005, July 2018. doi: 10.1088/1361-6587/aad252.

[2] Patrik Ollus, Scott Allan, James R Harrison, Andrew R Jackson, Taina Kurki-Suonio, Kenneth G McClements, Clive A Michael, David Moulton, Bhavin S Patel, Michael Robson, et al. Validating the simulation of beam-ion charge exchange in MAST Upgrade. *Plasma Physics and Controlled Fusion*, 2023.

[3] J Lovell, Matthew L Reinke, AR Field, Bartosz A Lomanowski, and MAST Upgrade Team. Overview and first measurements of the mast upgrade bolometer diagnostic. *Review of Scientific Instruments*, 94(2), 2023.

[4] GF Matthews, P Bunting, S Devaux, P Drewelow, C Guillemaut, DB King, E Lerche, S Silburn, G Szepesi, V Riccardo, et al. Energy balance in JET. *Nuclear Materials and Energy*, 12:227–233, 2017.

[5] Patrik Ollus, R Akers, B Colling, H El-Haroun, D Keeling, Taina Kurki-Suonio, R Sharma, Antti Snicker, Jari Varje, et al. Simulating the impact of charge exchange on beam ions in MAST-U. *Plasma Physics and Controlled Fusion*, 64(3):035014, 2022.

[6] C A Michael, N Conway, B Crowley, O Jones, W W Heidbrink, S Pinches, E Braeken, R Akers, C Challis, M Turnyanskiy, A Patel, D Muir, R Gaffka, and S Bailey. Dual view FIDA measurements on MAST. *Plasma Physics and Controlled Fusion*, 55(9):095007, jul 2013.

[7] AR Jackson, AS Jacobsen, KG McClements, CA Michael, and Marco Cecconello. Diagnosing fast ion redistribution due to sawtooth instabilities using fast ion deuterium-α spectroscopy in the mega amp spherical tokamak. *Nuclear Fusion*, 60(12):126035, 2020.

[8] Garrett Prechel, Nicolas Fil, Deyong Liu, WW Heidbrink, Clive Michael, Andrew Robert Jackson, MAST-U Team, et al. Installation of a solid state neutral particle analyzer array on mega ampere spherical tokamak upgrade. *Review of Scientific Instruments*, 93(11), 2022.

[9] C Vincent, S Allan, G Naylor, R Stephen, S Bray, A Thornton, and A Kirk. Fission chamber data

acquisition system for neutron flux measurements on the Mega-Amp Spherical Tokamak Upgrade. *Review of Scientific Instruments*, 93(9):093509, 2022.

[10] Marco Cecconello, IJ Dolby, Andrea Sperduti, J Rivero-Rodriguez, Göran Ericsson, I Fitzgerald, SY Allan, J Voller, B Honey, BA Nizar, et al. First observations of confined fast ions in mast upgrade with an upgraded neutron camera. *Plasma Physics and Controlled Fusion*, 65(3):035013, 2023.

[11] A. Pankin, D. McCune, R. Andre, G. Bateman, and A Kritz. The tokamak Monte Carlo fast ion module NUBEAM in the National Transport Code Collaboration library. *Computer Physics Communications*, 159(3):157–184, 2004.

[12] R.J. Goldston, D.C. McCune, H.H. Towner, S.L. Davis, R.J. Hawryluk, and G.L. Schmidt. New techniques for calculating heat and particle source rates due to neutral beam injection in axisymmetric tokamaks. *Journal of Computational Physics*, 43(1):61–78, September 1981. doi: 10.1016/0021-9991(81)90111-X.

[13] Jari Varje, Konsta Särkimäki, Joona Kontula, Patrik Ollus, Taina Kurki-Suonio, Antti Snicker, Eero Hirvijoki, and Simppa Äkäslompolo. High-performance orbit-following code ASCOT5 for Monte Carlo simulations in fusion plasmas. *arXiv preprint arXiv:1908.02482*, 2019.

[14] E. Hirvijoki, O. Asunta, T. Koskela, T. Kurki-Suonio, J. Miettunen, S. Sipilä, A. Snicker, and S. Äkäslompolo. ASCOT: Solving the kinetic equation of minority particle species in tokamak plasmas. *Computer Physics Communications*, 185(4):1310–1321, April 2014. doi: 10.1016/j.cpc.2014.01.014.

[15] F Militello, L Garzotti, J Harrison, JT Omotani, R Scannell, S Allan, A Kirk, I Lupelli, AJ Thornton, et al. Characterisation of the L-mode scrape off layer in MAST: Decay lengths. *Nuclear Fusion*, 56(1):016006, 2015.

[16] R Scannell, MJ Walsh, MR Dunstan, J Figueiredo, G Naylor, T O'Gorman, S Shibaev, KJ Gibson, and H Wilson. A 130 point Nd: YAG Thomson scattering diagnostic on MAST. *Review of Scientific Instruments*, 81(10):10D520, 2010.

[17] TL Rhodes, CA Michael, P Shi, R Scannell, S Storment, Q Pratt, R Lantsov, I Fitzgerald, VH Hall-Chen, NA Crocker, et al. Design elements and first data from a new Doppler backscattering system on the MAST-U spherical tokamak. *Review of Scientific Instruments*, 93(11), 2022.

[18] JC Hillesheim, NA Crocker, WA Peebles, H Meyer, A Meakins, AR Field, D Dunai, M Carr, N Hawkes, MAST Team, et al. Doppler backscattering for spherical tokamaks and measurement of high-k density fluctuation wavenumber spectrum in MAST. *Nuclear Fusion*, 55(7):073024, 2015.

[19] AR Field, J McCone, NJ Conway, M Dunstan, S Newton, and M Wisse. Comparison of measured poloidal rotation in MAST spherical tokamak plasmas with neo-classical predictions. *Plasma Physics and Controlled Fusion*, 51(10):105002, 2009.

[20] BD Dudson, N Ben Ayed, A Kirk, HR Wilson, G Counsell, X Xu, M Umansky, PB Snyder, B Lloyd, et al. Experiments and simulation of edge turbulence and filaments in MAST. *Plasma Physics and Controlled Fusion*, 50(12):124012, 2008.

[21] Otto Asunta, Joonas Govenius, Robert Budny, M Gorelenkova, Giovanni Tardini, Taina Kurki-Suonio, Antti Salmi, Seppo Sipilä, ASDEX Upgrade Team, et al. Modelling neutral beams in fusion devices: Beamlet-based model for fast particle simulations. *Computer Physics Communications*, 188:33–46, 2015.

[22] Brian LaBombard. KN1D: A 1-D space, 2-D velocity, kinetic transport algorithm for atomic and molecular hydrogen in an ionizing plasma. 2001. (Available at: https://dspace.mit.edu/handle/1721.1/93211).

[23] LC Johnson and EJ Hinnov. Ionization, recombination, and population of excited levels in hydrogen plasmas. *Journal of Quantitative Spectroscopy and Radiative Transfer*, 13:333, 1973.

[24] NJ Conway, PG Carolan, John Mccone, MJ Walsh, and Marco Wisse. High-throughput charge exchange recombination spectroscopy system on MAST. *Review of scientific instruments*, 77(10):10F131, 2006.

[25] Chris Bowman. `https://github.com/C-bowman/pedestal-inference`. Accessed: April 29, 2024.

[26] LL Lao, H St John, RD Stambaugh, AG Kellman, and W Pfeiffer. Reconstruction of current profile parameters and plasma shapes in tokamaks. *Nuclear Fusion*, 25(11):1611, 1985.

[27] LC Appel, GTA Huysmans, LL Lao, PJ McCarthy, DG Muir, ER Solano, J Storrs, D Taylor, W Zwingmann, et al. A unified approach to equilibrium reconstruction. In *Proceedings-33rd EPS conference on Controlled Fusion and Plasma Physics, pp. P–2.160*, 2006.

[28] HP Summers, WJ Dickson, MG O'mullane, Nigel R Badnell, AD Whiteford, DH Brooks, J Lang, SD Loch, and DC Griffin. Ionization state, excited populations and emission of impurities in dynamic finite density plasmas: I. The generalized collisional–radiative model for light elements. *Plasma Physics and Controlled Fusion*, 48(2):263, 2006.